Epoxidation of unfunctionalized olefins by Mn(salen) catalyst using organic peracids as oxygen source: A theoretical study

Ilja V. Khavrutskii, Djamaladdin G. Musaev*, and Keiji Morokuma*

Cherry L. Emerson Center for Scientific Computation and Department of Chemistry, Emory University, Atlanta, GA 30322

Edited by Barry M. Trost, Stanford University, Stanford, CA, and approved February 26, 2004 (received for review October 31, 2003)

The mechanism and origin of asymmetric induction in the Mn^{III}(salen)-catalyzed epoxidation by peracetic acid have been elucidated by the density functional [Becke three-parameter hybrid functional combined with Lee–Yang–Parr correlation functional (B3LYP)] method in two different regimes: with and without an axial ligand. The acylperoxo complexes of $Mn^{II,III,IV}$ in *cisON cisNO* and *trans* geometrical configurations cannot compete with the catalyst-free Prilezhaev epoxidation. Instead, oxo species perform epoxidation following the O–O bond cleavage in the acylperoxo complexes. The epoxidation may proceed in a concerted and/or radical-mediated stepwise manner. The actual mechanism of the epoxidation depends on the electronic and oxidation state of the oxo species and the nature of the axial ligand. The olefin can approach the reactive MnO fragment of both *cis* and *trans*-L-isomers of the plain oxo species along multiple distinct directions: native approaches. The native approaches are used to rationalize the inversion of the absolute configuration of the product epoxide due to the axial ligand.

Highly enantioselective Kochi–Jacobsen–Katsuki epoxidation of unfunctionalized olefins with Mn^{III}(salen)-based chiral catalyst provides an efficient route to optically active epoxides (1–4). Understanding the mechanism of the epoxidation and the origin of asymmetric induction can lead to the development of new efficient catalysts and therefore is actively pursued (5–19). Numerous studies assume the Mn^{V}-oxo species postulated by Kochi and coworkers (20) to be the enantioselective oxidant. Although the Mn^{V}-oxo species has not been detected experimentally, its geometric and electronic structure, as well as the mechanism of the epoxidation, have been the focus of several theoretical investigations (5–11, 21–25).

The predicted electronic structure of the *trans*-Mn^{V}-oxo species is controversial due to small energetic differences between various electronic states. Without an axial ligand, the singlet, triplet, and quintet states of the square pyramidal complex are nearly degenerate. In the presence of axial ligands, the singlet state is strongly destabilized, whereas the triplet and quintet states remain nearly degenerate in energy. The mechanism of the epoxidation by the *trans*-Mn^{V}-oxo species has been predicted to depend on the spin state and presence of an axial ligand. Without an axial ligand, epoxidation is predicted to be concerted for the quintet and singlet states but stepwise (through a radical intermediate) for the triplet state (5, 6). Axial Cl^{-} ligand alters epoxidation by the quintet state from concerted to stepwise (5, 7–9).

The origin of the asymmetric induction is a separate issue from the epoxidation mechanism and is poorly understood (1–4, 11, 26–29). For the *trans*-Mn^{V}-oxo species, Jacobsen and Cavallo (11) and Houk *et al.* (28) computationally studied the asymmetric induction, describing only the small core part of the catalyst by quantum mechanics. To describe crucial noncovalent interactions between the olefin and the substituted salen, they used empirical force fields. Both agreed that olefin could approach the reactive MnO moiety in a side-on manner from multiple directions. However, Houk *et al.* (28) indicated olefin approach along the oxygen side of the salen ligand, whereas Jacobson and Cavallo (11) suggested a perpendicular approach to be the most favorable. Both studies demonstrated that olefin adds to the Mn^{V}-oxo species regioselectively, forming the most stable radical intermediate. Asymmetric induction by the *trans*-Mn^{V}-oxo species, besides the chiral C^{8}, $C^{8'}$ atoms, is believed to result from (*i*) catalyst twist due to the puckered $Mn(NC^{8}C^{8'}N')$ ring (28) and (*ii*) asymmetric fold along the NO edges of the catalyst due to the axial-ligand strain (23). Distortions of both types have been shown to increase the chirality content of the *trans*-Mn^{V}-oxo species (29).

Although the *trans*-Mn^{V}-oxo hypothesis can successfully explain most of the experimental data, in certain cases enantioselectivity depends on the oxygen source and reaction conditions, suggesting alternative oxygenating species (17, 18, 30–34). The most dramatic enantioselectivity variations are observed for a synthetically important class of oxidants, organic peracids (30–34). In particular, in the presence of *N*-alkyl imidazole or *N*-oxide axial ligands, high enantioselectivity is realized, whereas in the absence of axial ligands, either loss or most importantly inversion of the enantioselectivity occurs (30–34). The latter is tentatively attributed to the direct epoxidation by acylperoxo complexes of Mn^{III}(salen) (30–32). Despite recent experimental mechanistic studies of the Mn^{III}(salen)-catalyzed epoxidation by peracids, the nature of oxygenating species remains uncertain (14, 16–19, 35).

Here we computationally elucidate the mechanism of the catalytic epoxidation by peracids and elaborate the axial-ligand effect on the mechanism and enantioselectivity.

Computational Details

Because quantum mechanical studies on the epoxidation in the real system containing numerous bulky substituents on the salen catalyst and aryl-conjugated olefin are prohibitive, we used a chemically relevant model. Our model comprised fully conjugated salen catalyst in (*R*,*R*) conformation without any bulky substituents and ethylene as olefin probe. We used peracetic acid as an oxygen source. To study the axial-ligand effect we used imidazole (because it is known to enhance enantioselectivity of epoxidation) (30–32) and acetate (the natural by-product from the peracetic acid). We believe that this model should allow us to identify the true reactive species and adequately describe the mechanism of the epoxidation. Although it may be argued that no enantioselectivity can be achieved with such a model, we find that this model provides qualitative understanding of the origin of enantioselectivity, which can be elaborated further with more realistic models in the future.

All calculations were performed with the GAUSSIAN 03 program suite (36) with the density functional theory (DFT), specifically with the Becke three-parameter hybrid functional combined with Lee–Yang–Parr correlation functional (B3LYP) (37–39). Preference for

This paper was submitted directly (Track II) to the PNAS office.

Abbreviations: DFT, density functional theory; B3LYP, Becke three-parameter hybrid functional combined with Lee–Yang–Parr correlation functional.

*To whom correspondence may be addressed. E-mail: dmusaev@emory.edu or morokuma@emory.edu.

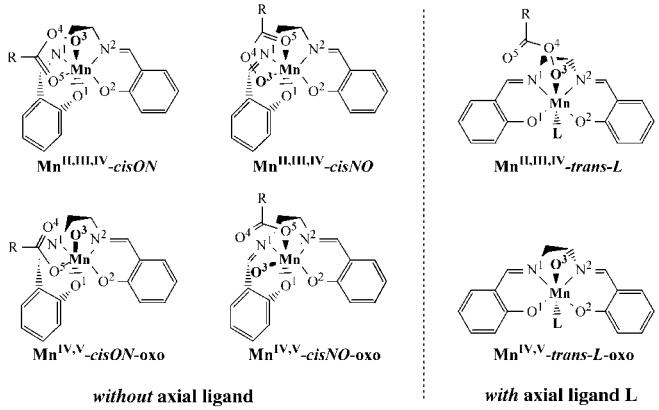

Fig. 1. Potential oxidants.

the B3LYP for the Mn(salen) systems has been justified in our recent studies (22, 40–42). Throughout this work we used a double-ζ LANL2DZ (BS1) (43) basis set with associated Hay–Wadt nonrelativistic effective core potential on Mn (44, 45) for geometry optimizations using the unrestricted B3LYP method.[‡] Unless otherwise stated, for the optimized structures we performed and used in discussion single-point energy calculations with triple-ζ quality basis set BS2, comprised of Stuttgart–Dresden basis set (8s7p6d1f)/[6s5p3d1f], with associated effective core potential on Mn (46), and 6-311+G(d) basis set (47) on the other atoms. Where applicable, spin contamination has been projected out by using the Yamaguchi approach (48, 49). Vibrational frequency calculations at the B3LYP/BS1 level have been performed only for the transition states to confirm their nature. Therefore, the energetics presented below does not include zero-point energy or entropy corrections.

Results and Discussion

The present study focuses on the Mn(salen)-catalyzed epoxidation of the ethylene by peracetic acid. For the reference, the barrier of the bimolecular catalyst-free Prilezhaev epoxidation by peracetic acid is calculated to be 16.4 kcal/mol ($\approx$17 kcal/mol in ref. 50). Thus, below we disregard the pathways of the Mn(salen)-catalyzed epoxidation, which depend on bimolecular elementary steps with barriers >17 kcal/mol.

The O–O Bond Cleavage in Mn(salen) Acylperoxo Complexes to Form oxo Complexes. Interaction of peracids with the chiral Mn(salen) catalyst produces a number of acylperoxo complexes of different geometric structure and oxidation state of the central Mn atom, as shown at the top of Fig. 1 (42). In Fig. 1 we use Mn^N–*cisYZ* and Mn^N–*trans*-L notation, where *Y* and *Z* stand for the atoms of the salen ligand situated trans to peroxo oxygen and carbonyl oxygen of the acylperoxo ligand, respectively, L represents an exogenous ligand, and N reflects the oxidation state of the Mn. The most important geometric isomers are *trans*, *cisON*, and *cisNO* and the oxidation states are II, III, and IV. These acylperoxo complexes can produce various oxo species via O–O bond cleavage, as discussed below and summarized in Fig. 1.

Mn^{II} complexes. Mn^{II}–acylperoxo complexes cleave the O–O bond to produce exclusively Mn^{IV}-oxo species. The lowest barriers on the ground sextet-state potential energy surface in the absence of an axial ligand are 14.6 and 17.3 kcal/mol for *cisON* and *cisNO* isomers, respectively. With the axial NH_3 ligand (model of imidazole), the barrier is 16.6 kcal/mol in Mn^{II}–*trans*-NH_3. The relative energies of the product Mn^{IV}–*cisON*, –*cisNO*, and –*trans*-NH_3 oxo species in the ground quartet state are −9.7, −12.8, and −25.3 kcal/mol, suggesting a spin crossover during the reaction.

Mn^{III} complexes. The O–O bond cleavage in Mn^{III}–acylperoxo complexes has been discussed elsewhere (41, 42). In summary, in the absence of axial ligand the O–O bond cleaves via a quintet-triplet spin-crossover pathway with overall 16.5 and 18.4 kcal/mol activation for the *cisON* and *cisNO* isomers to produce corresponding Mn^V–*cis*-oxo species in the triplet state, with relative energies of 2.6 and 2.0 kcal/mol, whereas formation of *trans*-oxo species is unfavorable.

In the presence of the axial ligand L = NH_3 and HCO_2^- (models of imidazole and acetate), the O–O bond of the Mn^{III}–*trans*-L-acylperoxo complexes cleaves with overall 13.7 and 12.4 kcal/mol activation energy to produce chameleon *trans*-L-oxo species with 8.4 and 5.6 kcal/mol relative energies. By "chameleon" we imply that product *trans*-oxo species can be regarded as either associated Mn^{IV}–*trans*-L-oxo and RCO_2 radical or Mn^V–*trans*-L-oxo and RCO_2 anion.

Mn^{IV} complexes. The Mn^{IV}–acylperoxo complexes in their ground quartet state are inert to the O–O bond cleavage and consequently have been characterized by ESR (14–16, 19), UV/visible, Raman, extended x-ray absorption fine-structure, and x-ray absorption near-edge spectroscopies (12).

Potential oxidants for olefin epoxidation. The acylperoxo complexes may participate in the olefin epoxidation directly or through various oxo species. Fig. 1 depicts all potential oxidants in the presence and absence of axial ligands.

Although our calculations show formation of the square pyramidal Mn^V–*trans*-oxo species to be impractical (42), this hypothetical "naked" oxo species helps to appreciate the axial-ligand effect and has been studied theoretically (5, 6, 22–25). The ground state of the Mn^V–*trans*-oxo species has been predicted to be singlet, triplet, or quintet. An axial ligand L such as imidazole or acetate destabilizes the singlet state of the octahedral Mn^V–*trans*-L-oxo by 12–13 kcal/mol, leaving either triplet or quintet as the ground state (22). Furthermore, the axial ligand changes the triplet state with two α electrons localized mainly on Mn to the triplet state with three α on Mn and one β on O^3, the antiferromagnetic analog of the quintet state. Energy-wise, the triplet state for the acetate and imidazole is 1.3 kcal/mol lower and 0.3 kcal/mol higher than the quintet, respectively. Similar effects have been reported for acetonitrile and *N*-oxide axial ligands (23). Because the four unpaired electrons in the triplet and quintet states reside in similar orbitals and only differ by spin coupling, (22) we suppose that both states would have similar reactivity. Therefore, below we discuss the epoxidation mechanism by Mn^V–*trans*-L-oxo species in the quintet state.

The Mn^V–*cis*-oxo species have a triplet ground state. Similar to the triplet state of Mn^V–*trans*-L-oxo species the *cis* oxo species have three α electrons on Mn and one β electron on O^3 (22, 42). However, the energy difference between the antiferromagnetic triplet and ferromagnetic quintet states in the *cis* oxo species is substantially larger than in the *trans* case. In particular, the quintet states of the *cisON* and *cisNO* oxo species are 4.6 and 7.3 kcal/mol higher than the corresponding triplet states. Despite high relative energy, the epoxidation by the quintet *cis* oxo species is of considerable interest, because the final complex of the Mn^{III}(salen)L with the epoxide has the quintet ground state (22).

The Mn^{IV}–*trans*-L-oxo species with and without an axial ligand as well as the Mn^{IV}–*cis*-oxo species have quartet ground states. The lowest doublet and sextet states are substantially higher ($\approx$7–17 kcal/mol) even in the absence of an axial ligand (22). Therefore, we consider only quartet ground state in the epoxidation.

Below, we study the epoxidation by acylperoxo and oxo complexes, respectively.

[‡]The table of Cartesian coordinates for all transition-state structures is available on request.

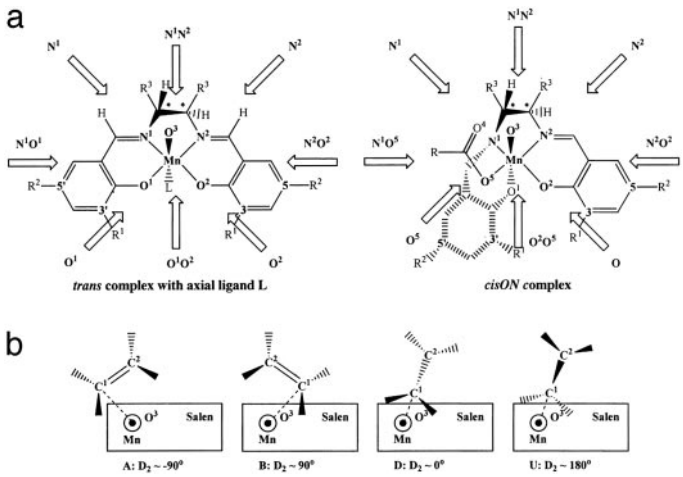

Fig. 2. Notation used to describe olefin approaches to the reactive MnO^3 fragment (*A*) and olefin orientations with D_2, the dihedral angle $MnO^3C^1C^2$ (*B*). In *A*, the *cisNO* isomer is not shown for brevity.

Epoxidation by Acylperoxo Complexes. Here we discuss direct epoxidation of the ethylene by acylperoxo complexes. Fig. 2 introduces the notation for olefin approaches to the reactive MnO^3 fragment. We label the approaches as K_M, where K is N^1, N^2, O^1, O^2, or O^5 and is used to designate the orientation of the O^3–C^1 vector along the salen molecule. The C^1 is the ethylene carbon atom forming the bond with O^3. Two letters, such as N^1N^2, are used for K to represent the midpoint between the two atoms. The label M is A(−90°), B(90°), D(0°), or U(180°), and reflects the $MnO^3C^1C^2$ dihedral angle (in parentheses) to specify orientation of the olefin along the approach vector O^3–C^1.

Epoxidation by acylperoxo complexes in the absence of axial ligand. For each geometric isomer and each oxidation state of *cis* acylperoxo complexes in the corresponding ground spin state, we found structurally similar transition states with olefin approaching in a side-on fashion with B orientation, namely O^2_B for *cisON* and O^1O^2_B for *cisNO*, as summarized in Fig. 3.

Following the reaction coordinate from the transition states to the products indicates that the epoxidation by acylperoxo complexes in the ground spin states is asynchronous (O^3C^1 distance is shorter than O^3C^2, as seen in Fig. 3) concerted, regardless of the oxidation state. However, because these epoxidation pathways are bimolecular with barriers >17 kcal/mol, they are unlikely to compete with Prilezhaev epoxidation.

The transition states for the epoxidation by *trans*-acylperoxo complexes in the high spin states seem to have higher barriers than for the *cis*-acylperoxo complexes and have been discarded.

We also sought epoxidation transition states by the Mn^{III}–*cis*-acylperoxo complexes in the low-lying excited triplet state, which is the most reactive in the O–O cleavage. However, instead of direct epoxidation we found olefin assisted O–O bond cleavage transition states producing *cis* oxo species with 14.9 and 17.2 kcal/mol barriers for *cisON* and *cisNO* isomers, respectively. These barriers are lower than in the absence of the olefin (16.5 and 18.4 kcal/mol, respectively).

Epoxidation in the presence of an axial ligand. We do not discuss direct epoxidation by the *trans*-L-acylperoxo complexes, because in the presence of the axial ligand the O–O bond cleavage has overall 12.4–13.7 kcal/mol activation energy even without the substrate assistance (41). Thus, *trans*-L-acylperoxo complexes should effectively convert to the *trans*-L-oxo species.

In brief, direct epoxidation by acylperoxo complexes in any oxidation state cannot compete with catalyst-free Prilezhaev epoxidation. On the other hand monomolecular O–O bond cleavage in Mn^{II}– and Mn^{III}–*cis* and –*trans*-L-acylperoxo complexes to produce corresponding oxo species is facile. Therefore, below we investigate epoxidation by the oxo species.

Epoxidation by oxo Complexes. Here we elucidate the epoxidation mechanism by various oxo species. We first address epoxidation by Mn^V–*cis*-oxo species (potential oxidants in the absence of axial-ligand) and then discuss epoxidation by Mn^V- and Mn^{IV}–*trans*-L-oxo species (potential oxidants in the presence of axial ligand). To elaborate the axial-ligand effect on the enantioselectivity we compare the latter case with Mn^V–*cis*- and hypothetical *trans*-oxo species without axial ligands.

Epoxidation by* cis*-oxo complexes. In the preceding paragraph we assumed that the pattern of reactivity for quintet ferromagnetic and triplet antiferromagnetic states of the Mn^V-oxo species should be alike due to similarity of the electronic structure. We verify this assumption by studying both spin states rigorously, although quintet *cis* oxo species should not contribute to enantioselectivity (42). Table 1 summarizes all transition states optimized with a variety of olefin approaches and orientations for the Mn^V–*cis*-oxo complexes, in the quintet and triplet states, with their important geometrical parameters, imaginary vibrational frequencies, and relative energies. Recall that the relative energies of the triplet and quintet states of *cisON*-oxo species are 2.6 and 7.2 kcal/mol, whereas those of *cisNO*-oxo species are 2.0 and 9.3 kcal/mol, respectively.

The *cisON*-oxo species resembles *trans*-L-oxo species in orientation of the reactive MnO^3 fragment and is discussed first. For the quintet-state *cisON*-oxo species we found two pairs of pseudosymmetric side-on approaches {O^5_A; O^2_B} and {O^5_B; O^2_A}, as shown in Table 1. The carboxylate ligand in the *cisON* oxo species is not involved in any hydrogen bonding with the chiral diimine bridge and readily interacts with the incoming olefin, which results in large differentiation within pairs of pseudosymmetric approaches. Specifically, the quintet energies for {O^5_A; O^2_B} and {O^5_B; O^2_A}, respectively, are {13.6; 16.2} and {13.8; 17.0} kcal/mol relative to the quintet *cisON*-acylperoxo complex.

For the triplet-state *cisON*-oxo, as expected, we found approaches {O^2O^5_A; O^2_B} and {O^5_B; O^2_A} similar to those of the quintet state. However, the relative energies of these transition states, {7.6; 6.9} and {7.2; 7.5} kcal/mol, are substantially lower than those of the quintet states. Surprisingly, the energy differences within the triplet-state pairs are qualitatively different from the quintet case. This finding suggests that spin state may actually affect the enantioselectivity of the epoxidation.

The *cisNO*-oxo species is very different from the *cisON* and *trans*-L-oxo species. The most prominent feature of the *cisNO*-isomer is that the reactive MnO^3 fragment is coplanar to both nitrogen atoms of the chiral diimine bridge and is consequently remote from the chiral centers (see Fig. 1). Furthermore, the carboxylate ligand forms a hydrogen bond with one of the chiral centers of the diimine bridge. Perhaps the most important feature is that the O^1N^1 side phenyl ring is bent toward the MnO^3 fragment

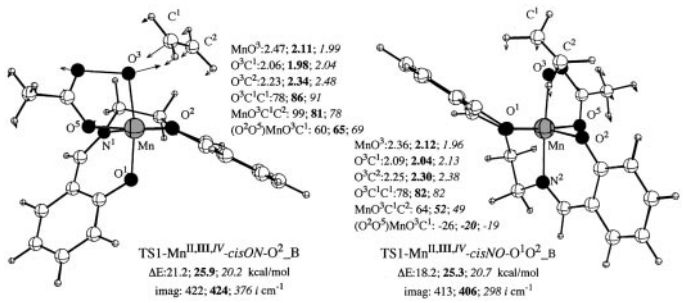

Fig. 3. Transition states TS1-$Mn^{II,III,IV}$–*cisON*-O^2_B and TS1-$Mn^{II,III,IV}$–*cisNO*–O^1O^2_B for direct epoxidation by cis acylperoxo complexes. Bond distances are in Å, and bond and dihedral angles are in degrees.

Table 1. Transition states for epoxidation (TS1) with different ethylene approaches and orientations obtained for Mn^{V}–*cis*-oxo complexes

Mn^{N}-state–isomer	K_M	ΔE	Imag	D_1	MnO^3	O^3C^1	O^3C^2	A_1	D_2
Mn^{V}–^{5}A–*cisON*	O^2_B	16.2	203i	41	1.86	2.20	2.80	101	90
	O^2_A	17.0	67i	34	1.86	2.57	2.78	84	−68
	O^5_B	13.8	180i	−47	1.84	2.19	2.76	99	66
	O^5_A	13.6	176i	−35	1.84	2.20	2.77	99	−106
Mn^{V}–^{3}A–*cisON*	O^2_B	6.9	111i	39	1.78	2.23	2.76	98	91
	O^2_A	7.5	70i	40	1.78	2.46	2.60	80	−76
	O^5_B	7.2	51i	−22	1.79	2.68	2.84	83	53
	O^2O^5_A	7.6	52i	5	1.79	2.34	2.79	94	−121
Mn^{V}–^{5}A–*cisNO*	O^5_U	16.6	240i	141	1.82	2.19	2.82	102	174
	N^1O^5_A	14.8	203i	166	1.82	2.18	2.74	99	−93
	O^1O^2_B	17.0	220i	−11	1.83	2.17	2.75	99	37
	O^1O^2_A	15.9	242i	4	1.82	2.19	2.78	100	−133
Mn^{V}–^{3}A–*cisNO*	N^1O^5_B	9.9	238i	−179	1.77	2.12	2.74	101	104
	N^1O^5_A	7.7	145i	165	1.76	2.20	2.72	97	−90
	O^1O^2_B	5.9	106i	18	1.75	2.26	2.79	98	143
	O^1O^2_A	6.4	47i	32	1.76	2.56	3.10	100	−113

ΔE (kcal/mol): B3LYP/BS2//B3LYP/BS1 energy of TS1 relative to separated substrate and Mn^{III}–*cisON* acylperoxo complex in the quintet state (see text for the relative energies of the *cis* oxo species); Imag (cm^{-1}), imaginary vibrational frequency; dihedral angle D_1 = $(O^1O^2)MnO^3C^1$, D_2 = $MnO^3C^1C^2$; bond angle A_1 = $O^3C^1C^2$; distances are in Å, and angles are in degrees.

such that it completely prevents side-on olefin approach from the O^1N^1 side (see Fig. 1). Last, the alkyl group R of the carboxylate is very close to the MnO^3 fragment and provides additional restrictions to the olefin approach, which effectively divides the approaches into two groups, one from the O^1O^2 side and the other from the N^1O^5 side.

For the quintet-state *cisNO*-oxo species we found two pseudosymmetric pairs of olefin approaches, {O^1O^2_A; O^1O^2_B} and {N^1O^5_A; O^5_U}, shown in Table 1. The relative energies of these transition state are {15.9; 17.0} and {14.8; 16.6} kcal/mol, respectively. Similar to the *cisON*, several hydrogen bonds are involved in latching the olefin.

For the triplet-state *cisNO* species we found similar pairs of transition states {O^1O^2_A; O^1O^2_B} and {N^1O^5_A; N^1O^5_B}. The energies for these pairs are {6.4; 5.9} and {7.7; 9.9} kcal/mol, respectively.

The most favorable epoxidation transition states for both triplet *cis* oxo species have the olefin in the B orientation. Although triplet-state *cisON*- and *cisNO*-oxo species have comparable relative energies for epoxidation, the barrier for the formation of the *cisNO* oxo species is 1.9 kcal/mol higher than for *cisON*, suggesting that *cisNO* species might be less important in the epoxidation.

Epoxidation by* trans-*L-oxo complexes. In the presence of axial ligands the O–O bond cleavage results in the chameleon *trans*-L-oxo species, which acts as either Mn^{V}– or Mn^{IV}–*trans*-L-oxo species depending on the axial ligand and reaction conditions (41). Here we investigate the asymmetric induction step by isolated Mn^{V}– and Mn^{IV}–*trans*-L-oxo species with L = imidazole and acetate.

For the quintet-state Mn^{V}–*trans*-L-oxo species we find that with neutral axial ligand imidazole, the epoxidation is asynchronous (O^3C^1 and O^3C^2 distances differ by as much as 0.7 Å) concerted, whereas with the anionic acetate, the reaction switches to a stepwise (forming Mn^{IV} radical intermediate) mechanism. The latter agrees with previous studies on a smaller model with axial ligand Cl^- (5, 7–9). The epoxidation by Mn^{V}–*trans*-L-oxo species in the triplet spin state is stepwise regardless of the axial ligand.

We located two pairs of perfectly side-on pseudosymmetric olefin approaches, {O^1_B; N^2O^2_A}, {O^1_A; O^2_B}, for the quintet Mn^{V}–*trans*-L oxo with both ligands, as seen in Table 2. The energy differences within the pairs of olefin approaches with axial ligands are 0.6–0.9 kcal/mol even for ethylene, which is an increase from 0.1 kcal/mol for the hypothetical naked Mn^{V}–*trans*-oxo species (refer to Table 3, which is published as supporting information on the PNAS web site). Because the ethylene in all the transition states samples only one phenyl ring at a time, the only explanation to the increase in the energy difference is the folding of the catalyst along the NO edges due to the axial ligand. With the axial ligand, the N^2O^2 side phenyl ring is bent upward, disfavoring olefin approaches along that side. This finding supports the suggestion that asymmet-

Table 2. Transition states for epoxidation (TS1) with different ethylene approaches and orientations obtained for $Mn^{IV,V}$–*trans*-L oxo complexes

Mn^{N}-state–L	K_M	ΔE	Imag	D_1	MnO^3	O^3C^1	O^3C^2	A_1	D_2
Mn^{V}–^{5}A–imidazole[†]	N^2O^2_A	3.6 (5.9)	203i	83	1.79	2.17	2.78	101	−83
	O^1_A	1.9 (3.7)	99i	−43	1.80	2.31	2.92	102	−89
	O^2_B	2.5 (4.3)	176i	45	1.79	2.19	2.83	103	94
	O^1_B	3.0 (5.0)	92i	−61	1.81	2.40	2.70	87	82
Mn^{IV}–^{4}A	O^1O^2_A	18.7 (18.2)	575i	−2	1.78	1.93	2.69	107	−105
	N^1_A	23.7 (23.2)	655i	−162	1.78	1.84	2.69	111	−81
	O^1O^2_B	18.5 (18.1)	571i	−9	1.78	1.92	2.69	107	109
	N^2_B	24.2 (22.6)	666i	130	1.79	1.82	2.69	113	69

ΔE (kcal/mol): B3LYP/BS2//B3LYP/BS1 energy of TS1 relative to separated substrate and Mn–*trans*-L-oxo species in high-spin state; Imag (cm^{-1}), imaginary vibrational frequency; dihedral angle D_1 = $(O^1O^2)MnO^3C^1$; D_2 = $MnO^3C^1C^2$; bond angle A_1 = $O^3C^1C^2$; distances are in Å, and angles are in degrees.

[†]Energy in parentheses is for L = acetate.

ric folding may enhance the enantioselectivity of the epoxidation (23, 29).

For the quartet ground state of Mn^{IV}–*trans*-L-oxo species epoxidation is asynchronous stepwise regardless of the axial ligand. For Mn^{IV}–*trans*-L-oxo species we also found two pseudosymmetric pairs of approaches, {O^1O^2_A; O^1O^2_B} and {N^2_B; N^1_A}; however, these approaches are drastically different from those of Mn^{V}–*trans*-L-oxo species. Although approaches {O^1O^2_A; O^1O^2_B} sampling the twist of the phenyl rings have the lowest energy, the energy difference between the two is extra small (0.2 kcal/mol). On the other hand, the approaches {N^1_A; N^2_B}, which sample the asymmetric diimine bridge, have an energy difference of 0.5–0.6 kcal/mol, which is comparable with the energy induced by the bend in the catalyst observed in Mn^{V}–*trans*-L-oxo species. Note that, because epoxidation by the Mn^{IV}–*trans*-L-oxo species is a bimolecular reaction with the activation energies >18 kcal/mol, it should not contribute to enantioselectivity. For the same reason, we do not discuss epoxidation by Mn^{IV}–*cis*-oxo species.

In contrast to Mn^{V}–*cis*-oxo species, the most favorable epoxidation transition states for the Mn^{V}–*trans*-L-oxo species have the olefin approach in the A orientation. Taking into account that substituted olefins add to MnO^3 regioselectively, the change of orientation from B to A due to axial ligand in our model corresponds to inversion of absolute configuration of epoxide with prochiral olefins.

Final Ring Closure of the Radical Intermediate. Let us briefly discuss the evolution of the system beyond the first transition state TS1 in the stepwise mechanism, which is relevant to the *cis-trans* scrambling of the epoxides and regeneration of the catalyst. The ring closure in the radical intermediate has been studied by others for Mn^{V}–*trans*-oxo species on smaller models (5–9).

Ring closure in the* cis*-oxo species. In the case of Mn^{V}–*cis*-oxo species, both quintet and triplet spin states form radical intermediates, with one unpaired electron on the C^2 atom coupled to three unpaired electrons on the Mn atom in ferromagnetic and antiferromagnetic fashion, respectively. Because the coupled electrons are well separated, the energies of these intermediates in both spin states are very similar. For the *cisON* intermediates the energies are −11.4 and −11.3 kcal/mol, whereas for the *cisNO* isomer they are −11.0 and −11.2 kcal/mol, in the quintet and triplet states, respectively. The transition state for the ring closure (TS2) is energetically higher for the triplet state, which is an indication of the spin crossover. In particular, for *cisON* the relative energies of the TS2 are −8.7 and −3.7 kcal/mol, whereas for *cisNO* they are −9.0 and −6.9 for the quintet and triplet states, respectively. The final product is the epoxide weakly coordinated to the Mn^{III}–*cis*-RCO_2^- salen complex. Here the difference between the quintet and triplet energies is the largest. Namely, for *cisON* and *cisNO* the relative energies of the quintet products are −34.8 and −37.3 kcal/mol, whereas those for the triplet products are −21.1 and −30.8 kcal/mol.

Ring closure in the* trans*-L-oxo species. For L = imidazole the reaction in the quintet state is concerted and leads directly to the epoxide with retention of the original stereoconfiguration. For the Mn^{V}–*trans*-L-oxo species with L = acetate, the Mn^{IV}–*trans*-L radical intermediates in the quintet and triplet states are −16.9 and −16.8 kcal/mol, respectively, and the ring closure TS2s are −14.7 for the quintet state and slightly higher −12.3 kcal/mol for the triplet state. The final product has stronger preference for the quintet state, which is −40.0 kcal/mol, whereas the triplet product is −31.6 kcal/mol.

Because epoxidation by Mn^{IV}–*trans*-L-oxo species is unlikely, we do not discuss the ring closure in the corresponding Mn^{III}–*trans*-L-radical intermediate. Nevertheless details of this transformation are provided in *Supporting Text*, which is published as supporting information on the PNAS web site.

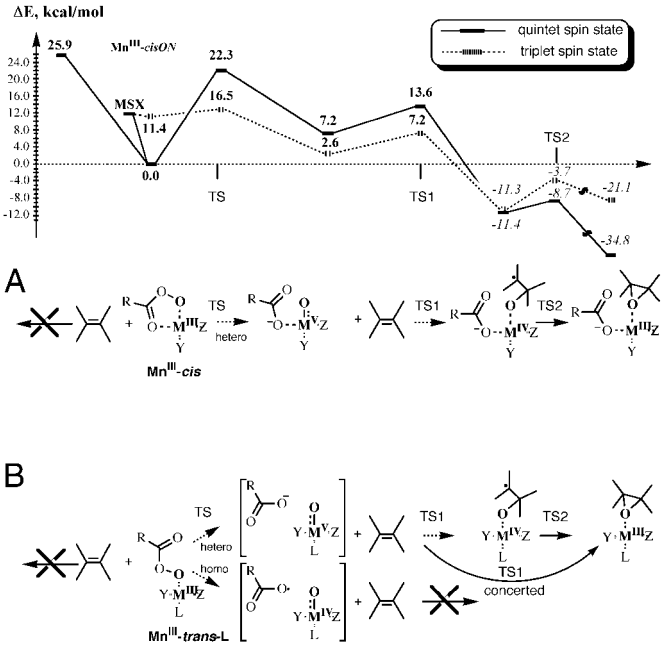

Fig. 4. The representative potential energy surface of Mn^{III}–*cisON* acylperoxo complexes, with the reaction mechanism in the absence (*A*) and presence (*B*) of axial ligands.

Concluding Remarks

To summarize, we have systematically studied the mechanism of the Mn^{III}(salen)-catalyzed epoxidation by peracids. We found that direct epoxidation by various acylperoxo complexes in three different oxidation states is unlikely because of higher activation energy than the noncatalyzed Prilezhaev epoxidation. Instead, the monomolecular O–O bond cleavage in the acylperoxo complexes occurs first, followed by epoxidation by the product oxo species. We find that only Mn^{V}–*cis*- and Mn^{V}–*trans*-L-oxo species can compete with the Prilezhaev reaction. The proposed reaction mechanism for epoxidation in the absence and presence of axial ligands is schematically drawn in Fig. 4 *A* and *B*, respectively. In addition, the top of Fig. 4*A* delineates a representative potential energy surface of the epoxidation reaction for the Mn^{III}–*cisON*-acylperoxo complex. Based on the activation energies we predict that the absolute rates for the O–O bond cleavage and subsequent epoxidation may be comparable depending on the concentrations of the catalyst, peracid, and olefin. To verify this prediction, experimental kinetics data on the epoxidation rates would be indispensable. Unfortunately, recent experimental mechanistic studies of the Mn^{III}(salen)-catalyzed epoxidation by peracids lack solid kinetics data due to very fast (within 1 min) epoxidation rates even at −78°C (14, 16–19, 35). Nevertheless, for closely related Mn^{III}(porphyrin) catalysts the rates of the Mn^{V} oxo species formation and/or subsequent epoxidation have been estimated in water and acetonitrile at room temperature and agree with our predictions (51, 52).

Importantly, we find that only for Mn^{V}–*trans*-L-oxo species with neutral imidazole axial ligand and only in the high-spin quintet state epoxidation proceeds in a concerted fashion with retention of original stereoconfiguration. In all other cases, epoxidation proceeds in a stepwise manner through an intermediate radical, potentially leading to *cis-trans* scrambling. Thus our results provide rationale for the experimentally observed sharp increase in the enantioselectivity of epoxidation of the terminal olefins by peracids at low temperature and in the presence of neutral axial ligand *N*-methylmorpholine-*N*-oxide (33–35). We explain that the domi-

nant active oxygenating species in that epoxidation at low temperature is quintet Mn^V–*trans*-L-oxo species with L = *N*-methylmorpholine-*N*-oxide, which epoxidizes terminal olefins concertedly by analogy with the L = imidazole case.

Besides the mechanism of the epoxidation, we addressed the origin of enantioselectivity in the epoxidation by reactive Mn^V–*cis* and Mn^V–*trans*-L-oxo species within the limits of our model. For all oxo species in all considered spin states, we found multiple approaches of the olefin to the reactive MnO^3 fragment. We call these approaches native, because our model is missing bulky substituents on the salen ligand and olefin substrate.

In the absence of an axial ligand the active oxygenating species are Mn^V–*cis*-oxo species, with the most favorable native olefin orientation being B, but in the presence of an axial ligand, the active oxygenating species change to Mn^V–*trans*-L with the most favorable olefin approach changed to A. Taking into account the fact that substituted olefins add to the MnO^3 fragment regioselectively, this provides an explanation to the experimentally observed inversion of the absolute configuration of the epoxidation due to axial ligands (30–32).

Additionally, comparison of the native approaches for Mn^V–*trans*-L and hypothetical naked Mn^V–*trans*-oxo species suggests that asymmetric folding of the salen ligand in Mn^V–*trans*-L-oxo species induced by the axial-ligand strain increases the energy difference within the pairs of pseudosymmetric approaches and might provide a guidelines for the choice of axial ligands to enhance enantioselectivity of epoxidation (23, 29).

Our unsubstituted model demonstrates that enantioselectivity of epoxidation for small alkenes by all considered oxo species is low. Also, available experimental data show that enantioselectivity of epoxidation of the small alkenes remains low even for the best-substituted salen catalysts. Consequently, it is reasonable to suppose that larger olefins show better enantioselectivity due to multiple interactions with the critical chirality regions of the catalyst. Thus, investigation of the asymmetric induction requires accurate description of the weak noncovalent interactions between the olefin and the substituted catalyst. One of such interactions is dispersion-type π–π interaction of the aryl-substituted olefins with the catalyst. In such case, the results from molecular mechanics or quantum mechanics/molecular mechanics studies on the subject must be taken with extra caution, because the dispersion interaction may not be described accurately. Even full DFT calculations will not be adequate, because the dispersion is not accounted for by DFT methods. An accurate description of the dispersion-type interaction in transition metal systems is a challenge and requires at least an MP2 level of theory. Nevertheless, it may be achieved with an ONIOM (MP2:DFT) approach (53). Therefore, the present work is essential for near-future investigations of the origin of the enantioselectivity with rigorous description of the crucial weak interactions.

This work was supported in part by National Science Foundation Grant CHE-0209660. We also acknowledge the use of computational resources of the Cherry L. Emerson Center of Emory University, supported in part by National Science Foundation Grant CHE-0079627 and an IBM Shared University Research Award.

1. Jacobsen, E. N. & Wu, M. H. (1999) in *Comprehensive Asymmetric Catalysis: Asymmetric Synthesis and Induction Catalysts*, ed. Yamamoto, H. (Springer, Berlin), Vol. 2, pp. 649–677.
2. Katsuki, T. (2001) *Curr. Org. Chem.* **5,** 663–678.
3. Katsuki, T. (2000) in *Catalytic Asymmetric Synthesis*, ed. Ojima, I. (Wiley–VCH, New York), pp. 287–325.
4. Jacobsen, E. N. (1993) in *Catalytic Asymmetric Synthesis*, ed. Ojima, I. (VCH, New York), pp. 159–202.
5. Abashkin, Y. G., Collins, J. R. & Burt, S. K. (2001) *Inorg. Chem.* **40,** 4040–4048.
6. Linde, C., Aakermark, B., Norrby, P.-O. & Svensson, M. (1999) *J. Am. Chem. Soc.* **121,** 5083–5084.
7. Cavallo, L. & Jacobsen, H. (2000) *Angew. Chem. Int. Ed. Engl.* **39,** 589–592.
8. Cavallo, L. & Jacobsen, H. (2003) *Eur. J. Inorg. Chem.* 892–902.
9. Cavallo, L. & Jacobsen, H. (2003) *J. Phys. Chem. A* **107,** 5466–5471.
10. Cavallo, L. & Jacobsen, H. (2003) *J. Org. Chem.* **68,** 6202–6207.
11. Jacobsen, H. & Cavallo, L. (2001) *Chem. Eur. J.* **20,** 1533–1544.
12. Feth, M. P., Bolm, C., Hildebrand, J. P., Kohler, M., Beckmann, O., Bauer, M., Ramamonjisoa, R. & Bertagnolli, H. (2003) *Chem. Eur. J.* **9,** 1348–1359.
13. Bryliakov, K. P., Babushkin, D. E. & Talsi, E. P. (2000) *Mendeleev Commun.* **1,** 1–3.
14. Bryliakov, K. P., Babushkin, D. E. & Talsi, E. P. (2000) *J. Mol. Catal. A Chem.* **158,** 19–35.
15. Bryliakov, K. P., Khavrutskii, I. V., Talsi, E. P. & Kholdeeva, O. A. (2000) *React. Kinet. Catal. Lett.* **71,** 183–191.
16. Bryliakov, K. P., Kholdeeva, O. A., Vanina, M. P. & Talsi, E. P. (2002) *J. Mol. Catal. A Chem.* **178,** 47–53.
17. Adam, W., Mock-Knoblauch, C., Saha-Moeller, C. R. & Herderich, M. (2000) *J. Am. Chem. Soc.* **122,** 9685–9691.
18. Adam, W., Roschmann, K. J., Saha-Moeller, C. R. & Seebach, D. (2002) *J. Am. Chem. Soc.* **124,** 5068–5073.
19. Campbell, K. A., Lashley, M. R., Wyatt, J. K., Nantz, M. H. & Britt, R. D. (2001) *J. Am. Chem. Soc.* **123,** 5710–5719.
20. Srinivasan, K., Michaud, P. & Kochi, J. K. (1986) *J. Am. Chem. Soc.* **108,** 2309–2320.
21. Jepsen, A. S., Roberson, M., Hazell, R. G. & Jorgensen, K. A. (1998) *Chem. Commun.*, 1599–1600.
22. Khavrutskii, I. V., Musaev, D. G. & Morokuma, K. (2003) *Inorg. Chem.* **42,** 2606–2621.
23. El-Bahraoui, J., Wiest, O., Feichtinger, D. & Plattner, D. A. (2001) *Angew. Chem. Int. Ed. Engl.* **40,** 2073–2076.
24. Plattner, D. A., Feichtinger, D., El-Bahraoui, J. & Wiest, O. (2000) *Int. J. Mass. Spectrom.* **195/196,** 351–362.
25. Strassner, T. & Houk, K. N. (1999) *Org. Lett.* **1,** 419–421.
26. Katsuki, T. (1995) *Coord. Chem. Rev.* **140,** 189–214.
27. Katsuki, T. (2002) *Adv. Synth. Catal.* **344,** 131–147.
28. Houk, K. N., DeMello, N. C., Condorski, K., Fennen, J. & Kasuga, T. (1996) *Proceedings of the ECHET96 Electronic Conference*. www.ch.ic.ac.uk/ectoc/echet96.
29. Lipkowitz, K. B. & Schefzick, S. (2002) *Chirality* **14,** 677–682.
30. Mukaiyama, T. & Yamada, T. (1995) *Bull. Chem. Soc. Jpn.* **68,** 17–35.
31. Imagawa, K., Nagata, T., Yamada, T. & Mukaiyama, T. (1994) *Chem. Lett.*, 527–530.
32. Yamada, T., Imagawa, K., Nagata, T. & Mukaiyama, T. (1994) *Bull. Chem. Soc. Jpn.* **67,** 2248–2256.
33. Palucki, M., Pospisil, P. J., Zhang, W. & Jacobsen, E. N. (1994) *J. Am. Chem. Soc.* **116,** 9333–9334.
34. Palucki, M., McCormick, G. J. & Jacobsen, E. N. (1995) *Tetrahedron Lett.* **36,** 5457–5460.
35. Palucki, M., Finney, N. S., Pospisil, P. J., Gueler, M. L., Ishida, T. & Jacobsen, E. N. (1998) *J. Am. Chem. Soc.* **120,** 948–954.
36. Frisch, M. J., et al. (2003) GAUSSIAN (Gaussian, Inc., Pittsburgh PA), Version 03.
37. Becke, A. D. (1988) *Phys. Rev. A At. Mol. Opt. Phys.* **38,** 3098–3100.
38. Becke, A. D. (1993) *J. Chem. Phys.* **98,** 5648–5652.
39. Lee, C., Yang, W. & Parr, R. G. (1988) *Phys. Rev. B Condens. Matter* **37,** 785–789.
40. Quiñonero, D., Musaev, D. G. & Morokuma, K. (2003) *Inorg. Chem.* **42,** 8449–8455.
41. Khavrutskii, I. V., Rahim, R. R., Musaev, D. G. & Morokuma, K. (2004) *J. Phys. Chem. B*, **108,** 3845–3854.
42. Khavrutskii, I. V., Musaev, D. G. & Morokuma, K. (2003) *J. Am. Chem. Soc.* **125,** 13879–13889.
43. Dunning, T. H. & Hay, P. J. (1977) in *Modern Theoretical Chemistry*, ed. Schaefer, H. F., III (Plenum, New York), Vol. 3, pp. 1–27.
44. Hay, P. J. & Wadt, W. R. (1985) *J. Chem. Phys.* **82,** 270–283.
45. Hay, P. J. & Wadt, W. R. (1985) *J. Chem. Phys.* **85,** 299–310.
46. Dolg, M., Wedig, U., Stoll, H. & Preuss, H. (1987) *J. Chem. Phys.* **82,** 866–872.
47. Krishnan, R., Binkley, J. S., Seeger, R. & Pople, J. A. (1980) *J. Chem. Phys.* **72,** 650–654.
48. Yamaguchi, K. (1988) *Chem. Phys. Lett.* **149,** 537–542.
49. Yamaguchi, K., Fukui, H. & Fueno, T. (1986) *Chem. Lett.*, 625–628.
50. Bach, R. D., Dmitrenko, O., Adam, W. & Schambony, S. (2003) *J. Am. Chem. Soc.* **125,** 924–934.
51. Groves, J. T., Lee, J. & Marla, S. S. (1997) *J. Am. Chem. Soc.* **119,** 6269–6273.
52. Zhang, R. & Newcomb, M. (2003) *J. Am. Chem. Soc.* **125,** 12418–12419.
53. Tschumper, G. S. & Morokuma, K. (2002) *Theochem* **592,** 137–147.